3C454.3 reveals the structure and physics of its 'blazar zone'.

Marek Sikora[1], Rafał Moderski[1], Greg M. Madejski[2,3]

ABSTRACT

Recent multi-wavelength observations of 3C454.3, in particular during its giant outburst in 2005, put severe constraints on the location of the 'blazar zone', its dissipative nature, and high energy radiation mechanisms. As the optical, X-ray, and millimeter light-curves indicate, significant fraction of the jet energy must be released in the vicinity of the millimeter-photosphere, i.e. at distances where, due to the lateral expansion, the jet becomes transparent at millimeter wavelengths. We conclude that this region is located at ~ 10 parsecs, the distance coinciding with the location of the hot dust region. This location is consistent with the high amplitude variations observed on ~ 10 day time scale, provided the Lorentz factor of a jet is $\Gamma_j \sim 20$. We argue that dissipation is driven by reconfinement shock and demonstrate that X-rays and γ-rays are likely to be produced via inverse Compton scattering of near/mid IR photons emitted by the hot dust. We also infer that the largest gamma-to-synchrotron luminosity ratio ever recorded in this object – having taken place during its lowest luminosity states – can be simply due to weaker magnetic fields carried by a less powerful jet.

Subject headings: galaxies: quasars: general — galaxies: jets — radiation mechanisms: non-thermal — gamma rays: theory — X-rays: general

1. Introduction

Multi-wavelength coverage of recent activity of quasar 3C454.3 provided exceptional data to investigate the structure and physics of its blazar zone. Prior to year 2000, this object spent most of its time in the low, relatively quiescent state. Starting in 2000, 3C454.3 entered a highly active state, changing optical flux by a factor tens on time scales of a few

[1]Nicolaus Copernicus Astronomical Center, Bartycka 18, 00-716 Warsaw, Poland; sikora@camk.edu.pl

[2]Stanford Linear Accelerator Center, 2575 Sand Hill Road, Menlo Park, CA 94025, USA

[3]Kavli Institute for Particle Astrophysics and Cosmology, Stanford University, Stanford, CA 94305

months (Fuhrmann et al. 2006; Villata et al. 2006). The most powerful event took place in the middle of 2005. This event was monitored also in the X-ray bands (Swift/XRT/BAT: Giommi et al. 2006; INTEGRAL: Pian et al. 2006; Chandra: Villata et al. 2006), and at millimeter wavelengths (Krichbaum et al. 2007).

These data allow a construction of quasi-simultaneous broadband spectrum around the outburst peak. As is the case for other blazars, the spectrum is composed of two humps, the lower energy one produced via synchrotron mechanism and peaking in the far-infrared band, and the higher energy one most likely generated by inverse-Compton process and peaking in the γ-ray band. The lack of coverage of the event by γ-ray observatories does not allow us to determine the luminosity of the high energy component. Nevertheless, X-ray data suggest that luminosity ratio of the high- to the low-energy components was much smaller during the outburst than during low states monitored in γ-rays by CGRO (Mukherjee et al. 1997; Hartman et al. 1999; Zhang et al. 2005).

This difference was theoretically investigated by Pian et al. (2006) and by Katarzyński & Ghisellini (2007). Pian et al. (2006) suggested that during the low states the blazar zone is located inside the broad line region (BLR) and that high energy spectra are produced by the External Radiation Compton (ERC) process involving scattering of broad line photons (via scenario described in Sikora et al. 1994), while during the 2005 outburst the dissipation zone moved outside the BLR where the ERC becomes inefficient. In such a model, production of the optical outburst doesn't require increase of a jet power. Similarly, in the scenario proposed by Katarzyński & Ghisellini (2007) the jet power is constant, but the drop of luminosity of the high energy component is explained by decrease of the Lorentz factor.

The idea of the constant jet power might be challenged by the most recent optical outburst which in July 2007 was also detected in γ-rays by AGILE (Vercellone et al. 2007). Bolometric luminosity of this outburst was 4-5 times larger than bolometric luminosity during the low optical states and the radiative output was strongly dominated by the γ-ray flux. The currently available millimeter-band light curves (Krichbaum et al. 2007) do not indicate any significant delay of the millimeter flux after the bolometric flux as inferred from the infrared and optical data presented in Bach et al. (2007). All of the above motivated us to investigate a different scenario, with the origin of the high energy peak involving ERC with IR seed photons and operating in the vicinity of the millimeter photosphere of the source. Basic assumptions of the scenario are described in §2; results of modeling of the broadband spectrum of the 2005 outburst are presented in §3; explanation of the large γ-ray dominance in the low optical states is provided in §4; and the main results are summarized in §5.

2. Model assumptions

2.1. Location of the blazar zone

Optical and millimeter light-curves show that the '2005 outburst' of 3C454.3 was actually preceded by a long term gradual increase in flux which started in August 2004 and continued until the middle of 2005 (Villata et al. 2006; Krichbaum et al. 2007). The optical flux reached maximum around May 9, then dropped very rapidly, but this drop was associated with several local "wiggles". The millimeter light-curve reached maximum about 18 days later and continued at that level for ~ 3 months with fluctuations on a time scale of ~ 10-days. The outburst ceased by the August/September 2005. The lack of a high luminosity plateau in the optical light curve suggests that the millimeter outburst lags the optical one by ~ 3 months. However no such long delay is seen in the growing part of the outburst. Furthermore, the optical spectrum is steep and very variable which makes the optical flux a very poor tracer of the *bolometric* luminosity. The latter, according to data presented by Bach et al. (2007), presumably reached the maximum (with the peak located in the far IR) by the end of June 2005, roughly in the middle of the millimeter plateau. This, coupled with large millimeter luminosities which require *in situ* energy dissipation rate that is comparable to the rate required to account for optical emission – and similar short term variability time scales in both spectral bands – suggest that regions of the optical and millimeter emission are not spatially detached.

If the above is indeed the case, it is possible to make unambiguous estimates of the location of the blazar zone (with respect to the central black hole) based on the variability time scales, and this in turn can be verified by using millimeter data and calculations of the synchrotron-self-absorption opacity of the source. Since the spectral slope measured in the millimeter band during the outburst is typically within the range $0.0 < \alpha_{mm} < 0.5$, the blazar zone is expected to be partially opaque at these wavelengths. The resulting size of the source R_{mm} and its distance from the center r_{mm} depend on the specific model parameters and for those presented in Table 1 are calculated to be $R_{mm} \sim 0.5$ pc and $r_{mm} \sim 9$ pc (see Appendix B).

2.2. Dissipation scenario

While it is relatively well-established that the endpoints of most quasar jets correspond to "hot spots" presumably involving terminal shocks, there is no consensus regarding the mechanism responsible for the energy dissipation within the flow and in particular in the blazar zone. Most popular, presumably because it is the easiest to treat quantitatively, is the

internal shock scenario. In accordance with this scenario, jets are radially inhomogeneous both in density and velocity and shocks are formed due to collisions between jet portions propagating with different Lorentz factors (Sikora et al. 1994; Spada et al. 2001). Internal shock scenario is attractive for blazars because predicts parallel polarization (electric vector position angle, EVPA, parallel to the jet) of the synchrotron radiation, in agreement with observations in the optical, infrared, and millimeter bands (Impey et al. 1991; Stevens et al. 1996; Nartallo et al. 1998; Jorstad et al. 2007). This prediction is independent of whether magnetic field is dominated by the toroidal component determined by poloidal electrical currents or by turbulent magnetic fields compressed in the transverse shocks (Laing 1981). However, internal shocks are known to dissipate energy very inefficiently: modulation of a jet Lorentz factor by at least a factor of 4 is required to reach a few percent of efficiency.

More promising dissipative scenario involves reconfinement shocks (Komissarov & Falle 1997; Sokolov et al. 2004). Such shocks keep pressure balance between the jet and its environment and are formed everywhere where density gradient of the external medium departs from the longitudinal density gradient in a jet. On sub-parsec scales the environment is too weak to affect dynamically powerful jets, but at parsec and larger distance, the interaction of the jet with its environment is sufficiently strong to modify the opening angle and, in the case of non-axisymmetric external matter density distribution, also the direction of propagation (see e.g. Appl et al. 1996). Reconfinement shock scenario provides interesting constraints on the structure and intensity of magnetic fields. In such shocks compression of chaotic magnetic fields leads to the perpendicular EVPA, but if magnetic field intensity is dominated by the toroidal component, the EVPA is parallel to the jet, in agreement with observations.

2.3. Radiative mechanisms and model input parameters

Basic radiative processes in relativistic jets are known to be the synchrotron mechanism and the inverse-Compton process. The latter involves scatterings of both 'internal' synchrotron photons (the SSC process) and 'external' photons (the ERC process). The ERC is expected to dominate strongly over the SSC provided radiative environment is strong and jets are highly relativistic (Dermer et al. 1992; Dermer & Schlickeiser 1993; Sikora et al. 1994; Blandford & Levinson 1995). At parsec distances, corresponding to the likely location of the blazar zone in 3C454.3 (see §2.1), the external diffuse radiation field is dominated by near/mid infrared radiation of hot dust (Cleary et al. 2007, and refs. therein) and therefore such dust is very likely to provide the dominant source of seed photons for the inverse-Compton process (Błażejowski et al. 2000; Arbeiter et al. 2002). This is in fact the scenario

suggested for the origin of the high-energy peak in MeV blazars (a class of blazars also encompassing 3C454.3; see Sikora et al. 2002) and is the scenario adopted below.

To reproduce the broadband spectrum of radiation produced in the blazar zone, we apply the numerical model BLAZAR (Moderski et al. 2003), updated for the treatment of the Klein-Nishina regime (Moderski et al. 2005). Originally, the model was designed to compute radiation spectra assuming the internal shock scenario, but noting that steady-state radiation can be superposed from a sequence of moving sources which all radiate within the same distance range, the model can be used also to approximate radiation production by the standing reconfinement shock.

Possibly the most significant simplification of our model is that we do not consider real geometry and kinematics of the reconfinement shock, adopting instead the uniform injection/acceleration of relativistic particles within the conically diverging zone. The details of the physics of reconfinement shocks and in particular of particle acceleration are still not known, and it is even unclear whether the dissipation process and particle acceleration involve just the reconfinement shock or some sort of a hybrid model incorporating internal shocks amplified in the reconfinement zone (Komissarov & Falle 1997; Sokolov et al. 2004).

The following input parameters are used in our model:

- radial extension of the blazar zone, Δr, and the distance of its inner edge from the center, r_0;
- the jet Lorentz factor, Γ_j, and its opening (half) angle θ_j;
- magnetic field intensity, $B = B_0 \times (r_0/r)$;
- the electron injection function, $Q = K\gamma^{-p}$ for $\gamma_{min} < \gamma < \gamma_{max}$;
- energy density of the diffuse component of hot dust radiation, $u_{IR} = u_{IR,in} \times [1 + (r/r_{in})^2]^{-1}$, where r_{in} is the inner edge of the hot dust region, $u_{IR,in} \sim \xi_{IR} L_{disk}/(4\pi r_{in}^2 c)$, L_{disk} is the accretion disk luminosity, and ξ_{IR} is the fraction of the disk radiation reprocessed by dust into infrared radiation;
- energy of the seed photons at thermal peak in νL_ν vs. ν diagram, $h\nu_{IR} \simeq 3.92\, kT$, where $T = T_{in}(r_{in}/r)^{1/2}$, and $T_{in} = (L_{disk}/(4\pi\sigma_{SB} r_{in}^2 c))^{1/4}$.

Values of these parameters are determined by our model assumptions and by relations between these parameters and observables. The latter, in the form of approximate formulas, are presented in Appendix A. Analytically estimated parameters are used to start an iterative

procedure to fit numerically the observed spectrum. Because the 2005 outburst was not observed in the γ-ray band and because of uncertainties regarding distribution and opacity of the hot dust, the set of input parameters cannot be determined uniquely. This in particular concerns the value of the jet Lorentz factor. We assumed $\Gamma_j = 20$. Such a large value allows us to avoid softening of the X-ray spectrum by contribution of the SSC process in the soft/mid X-ray bands. Such a large value of Γ_j is also implied when we adopt the assumption of domination of the toroidal magnetic component over the turbulent one. The $\Gamma_j = 20$ is larger than that deduced from the VLBI observations of the superluminal expansion (see Jorstad et al. 2001, and refs. therein), but the latter can be underestimated due to not taking into account effects of the divergence of a jet (Gopal-Krishna et al. 2006).

3. Modeling the 2005 outburst

Results of modeling of the spectrum observed in May 2005, when the optical flux was at its maximum are shown in Fig. 1 and input and output parameters are specified in Table 1. As it is apparent, the entire spectrum can be reproduced using a single-power-law for electron injection function, with a slope index $p = 2$. X-ray spectrum is produced by electrons which cool on a time scale longer than the blazar-zone crossing time and therefore this results in the slope $\alpha_X = (p-1)/2 \simeq 0.5$. Synchrotron spectrum is produced in the fast cooling regime and results in the slope $\alpha_{syn} = p/2 \simeq 1.0$, but in the optical band it significantly steepens due to high energy cutoff in the injection function. It hardens at the millimeter wavelengths due to synchrotron self-absorption.

Our results show that even a very moderate energy density of the dust radiation is sufficient to provide strong domination of the ERC luminosities over the SSC luminosities. This is due to a large value of Γ_j and strong dependence of the L_{ERC}/L_{SSC} ratio on Γ_j. The spectrum shown in Fig. 1 is obtained for an active zone enclosed within a distance range $10^{19} - 2 \times 10^{19}$ cm. Jet within this distance range is opaque at millimeter wavelengths.

In order to get spectrum with the observed slopes and fluxes in the millimeter band, it is necessary to assume a larger distance of the blazar zone and smaller optical luminosities. In Fig. 1 we show the broadband spectrum produced within a distance range $2 \times 10^{19} - 4 \times 10^{19}$ cm. Optical luminosity is smaller there by a factor ~ 5, but assuming that magnetic energy flux is proportional to the flux associated with matter flow, it was possible to accommodate this by decreasing the electron injection function by only a factor of 2 (see parameters in Table 1). Optical luminosity produced within this distance range corresponds with optical fluxes recorded during the millimeter-plateau period. Results from Fig. 1 indicate that most powerful portions of the jet start to dissipate energy closer to the

center than the less powerful ones, but energy dissipation extends, albeit with a decreasing efficiency, up to the region where the plasma becomes transparent at millimeter wavelengths.

4. Modeling different spectral states

Important observable characterizing the double-hump spectra of blazars is the luminosity ratio of the high energy component to the low energy component. If production of a high energy component is dominated by the ERC process, then this ratio is $L_{ERC}/L_{syn} \sim \Gamma_j^2 u_{IR}/u'_B$, where u'_B is energy density of the magnetic field in the blazar zone of a jet. Noting that energy flux of magnetic field in a jet is $L_B \simeq c u'_B \pi R^2 \Gamma_j^2$ and $u_{IR} = \xi_{IR} L_{disk}/(4\pi r^2 c)$, and assuming that $L_B \propto L_{jet}$ and $\theta_j = R/r \sim 1/\Gamma_j$, this ratio is

$$\frac{L_{ERC}}{L_{syn}} \propto \frac{\Gamma^2 \xi_{IR} L_{disk}}{L_{jet}} \tag{1}$$

Hence, for a fixed disk luminosity, luminosity ratio of the two components depends mainly on three parameters, Γ_j, ξ_{IR}, and L_{jet}. All of them can be a function of a distance in a jet, and Γ_j and L_{jet} can additionally vary with time. With our basic assumption that the blazar zone is related to the location of the reconfinement shock and that this location is not changing significantly with time, changes of the luminosity ratio from the epoch to the epoch can be just a function of L_{jet} and Γ_j. We demonstrate in Fig. 2 and 3 that spectra of 3C454.3 taken at two epochs, during the outburst and during the quiescent phase, can be reproduced just by assuming changes in L_{jet} and some modifications in the shape of the injection function. From inspection of these spectra (including Fig. 1), it is apparent that differences between synchrotron luminosities at different states are much larger than differences between bolometric luminosities. This results from the fact that for $L_{ERC} > L_{syn}$, $L_{ERC} \sim L_{bol} \propto L_{jet}$, and when this is combined with the Eq. (1), it gives $L_{syn} \propto L_{jet}^2$.

5. Discussion and conclusions

We demonstrated in this paper that broadband spectra of 3C454.3 can be reconstructed assuming that they are produced at distances $r \sim 3 - 9$ parsecs. By the end of this distance range the jet becomes transparent at millimeter wavelengths. Blazar activity historically has been defined via observations in the IR/optical bands, while "blazar-zone" is often considered to be located deeply within the millimeter photosphere. However, the optical and millimeter light-curves seem to indicate a significant overlap of the blazar-zone with a region where the jet becomes transparent at millimeter wavelengths (see §2.1). This is further supported by

very large millimeter luminosities which require high, *in situ*, dissipation rate of energy, and is consistent with time scales of the fastest high amplitude variations, of the order of 10 days in both spectral bands. Furthermore, at such distances the co-spatial model self-consistently incorporates production of X- and γ-rays, via scatterings of near/mid IR photons emitted by hot dust.

It should be emphasized here that the input-parameter set for ERC models is not unique and that high energy spectra can be reproduced also by scattering of broad emission photons if taking place in the sub-parsec region. However, then the high energy non-thermal radiation should be accompanied by bulk-Compton features (Sikora & Madejski 2000; Moderski et al. 2004; Celotti et al. 2007), which so far have not been observationally confirmed. Their lack or weakness can be explained by assuming that in the sub-parsec region jet is still in acceleration phase and the blazar zone is located at larger distances (Kataoka et al. 2007).

We identify the "blazar zone" with a reconfinement shock. That, together with optical polarization data imply domination of the toroidal magnetic field over chaotic/turbulent magnetic fields. However it should be noted that domination of the toroidal component doesn't necessary indicate the domination of the Poynting flux over the matter energy flux. It is very likely that the conversion of the Poynting flux dominated jet into matter dominated jet – and hence the jet acceleration process – are accomplished on sub-parsec scales (Sikora et al. 2005; Komissarov et al. 2007). Similar conclusions are reached by Jorstad et al. (2007), following multi-waveband polarimetric observations of 15 AGN.

During its 2005 outburst, 3C454.3 was the most luminous object ever recorded in the optical band. To explain such an outburst, the jet power larger than $7 \times 10^{47}\,\mathrm{erg\ s^{-1}}$ is required (see Table 1). Is it feasible? Noting that the estimates of the black hole mass in this object give $\sim 4 \times 10^9 M_\odot$ (Gu et al. 2001), we infer that the jet power is on the order of the Eddington luminosity. This, however, is at least by a factor of few larger than the accretion luminosity, which in turn, as determined from the optical luminosity of the thermal component detected during the low state (Smith et al. 1988), and after application of the bolometric correction, is likely to be of the order $10^{47}\,\mathrm{erg\ s^{-1}}$. 3C454.3 is in this respect not exceptional among most powerful radio-loud quasars: powers of jets larger than $10^{47}\,\mathrm{erg\ s^{-1}}$ have been inferred for several other quasars from analysis of the lobe energetics (Rawlings & Saunders 1991), as well as from Chandra and HST observations of gamma-ray blazars (Tavecchio et al. 2007).

This project was partially supported by Polish KBN grant 5 P03D 00221 and NASA observing grant NNX07AB05G. This work was also supported, in part, by the Department of Energy contract to SLAC no. DE-AC3-76SF00515. This research has made use of the

NASA/IPAC Extragalactic Database (NED) which is operated by the Jet Propulsion Laboratory, California Institute of Technology, under contract with the National Aeronautics and Space Administration.

A. Analytical approximations of the model parameters

A.1. Injection function

Normalization factor K_e of the electron injection function Q can be derived using approximate formulas for production of the X-ray spectrum via the ERC process in the slow cooling regime (see Moderski et al. 2003):

$$\nu_x L_{\nu_x} = \frac{1}{2}[\gamma N_\gamma]|\dot{\gamma}|_{ERC}(\theta_{obs}) m_e c^2 \mathcal{D}^4 \tag{A1}$$

where

$$|\dot{\gamma}|_{ERC}(\theta_{obs}) = \frac{c\sigma_T}{m_e c^2} u'_{IR} \gamma^2 \left(\frac{\mathcal{D}}{\Gamma_j}\right)^2 \tag{A2}$$

$$N_\gamma = Q\frac{\Delta r}{c\Gamma_j} \tag{A3}$$

$$u'_{ext} = \frac{4}{3}\Gamma_j^2 u_{ext} \tag{A4}$$

and

$$\mathcal{D} = \frac{1}{\Gamma_j(1-\beta\cos\theta_{obs})} \tag{A5}$$

In the slow cooling regime the slope p of the electron injection function is $p = 2\alpha_x + 1$ and for $\Delta r = r$ above equations give

$$K_e = \frac{3}{2}\frac{\nu_x L_{\nu_x}}{\sigma_T u_{IR} r}\frac{\Gamma_j}{\mathcal{D}^{4+2\alpha_x}}\left(\frac{\nu_{ext}}{\nu_x}\right)^{1-\alpha_x} \tag{A6}$$

In one of our models, the break in the injection functions is introduced in order to get a better fit of the observed spectrum:

$$Q = K_e \frac{1}{\gamma^p + \gamma_{br}^{p-q}\gamma^q} \tag{A7}$$

where γ_{br} is the break energy and q is the spectral index of the injection function at high energy limit.

A.2. Magnetic field intensity

The ERC to synchrotron peak luminosity ratio

$$\frac{L_{ERC}}{L_{syn}} = \frac{u'_{ext}(\mathcal{D}/\Gamma_i)^2}{u'_B} \tag{A8}$$

gives us magnetic field intensity

$$B' = \mathcal{D}\sqrt{\frac{32}{3}u_{ext}\frac{L_{ERC}}{L_{syn}}} \tag{A9}$$

and magnetic energy flux

$$L_B = cu'_B\pi R^2\Gamma_j^2 = \pi cu'_B r^2(\theta_j\Gamma_j)^2 \tag{A10}$$

where $u'_B = B'^2/(8\pi)$ is magnetic energy density. With known B' we can estimate the maximum energy of injected electrons

$$\gamma_{max} \simeq 5.2\times10^{-4}\sqrt{\frac{\nu_{syn,max,obs}(1+z)}{B'\mathcal{D}}} \tag{A11}$$

A.3. Electron energy density

Due to light travel effects, sources moving with relativistic speeds are seen on the sky as stretched by a factor $\mathcal{D}\Gamma_j$, which means that only a fraction $1/(\mathcal{D}\Gamma_j)$ of particles is seen at a given instance to be enclosed within the distance range Δr. Hence the volume of the jet segment into which electrons are injected at the 'observed' rate Q is $\pi R^2\lambda$, where $\lambda = \Delta r/(\mathcal{D}\Gamma_j)$. Amount of energy injected into the segment during its propagation through the Δr zone is

$$E'_{e,inj} = \frac{\Delta r}{c\Gamma_j}\int Q\gamma m_e c^2\, d\gamma \tag{A12}$$

and energy density of injected electrons is

$$u'_{e,inj}(r_0+\Delta r = 2r_0) = \frac{E'_{e,inj}}{\pi R^2\lambda'} = \frac{\mathcal{D}}{\Gamma_j}\frac{\int Q\gamma m_e c^2\, d\gamma}{\pi cR^2} = \frac{m_e c\mathcal{D}\Gamma_j\int Q\gamma\, d\gamma}{4\pi r_0^2(\theta_{obs}\Gamma_j)^2} \tag{A13}$$

where $\lambda' = \lambda\Gamma_j$.

A.4. Energy dissipation efficiency

In the proton inertia dominated jets acceleration of electrons is powered by protons and we have

$$u'_{e,inj} = \eta_e u'_p(\bar{\gamma}_p - 1) \tag{A14}$$

where $(\bar{\gamma}_p - 1) \ll 1$ is the fraction of proton bulk kinetic energy converted to the 'thermal' proton energy called hereafter the efficiency of energy dissipation, and η_e is the fraction of proton 'thermal' energy tapped by electrons. Condition of having matter dominated jet implies $u'_p > u'_B$, and combining this with previous equation gives

$$(\bar{\gamma}_p - 1) < \frac{u'_{e,inj}}{u'_B \eta_e} \tag{A15}$$

A.5. Pair content

Using definition of particle energy densities ($u = nmc^2\bar{\gamma}$) and noting that $\bar{\gamma} \gg 1$ (throughout our paper, $\gamma \equiv \gamma_e$) and $\bar{\gamma}_p - 1 \ll 1$ we obtain the pair content

$$\frac{n'_e}{n'_p} = \frac{m_p}{m_e}\frac{\bar{\gamma}_p - 1}{\bar{\gamma}} < \frac{m_p}{\eta_e \bar{\gamma} m_e}\frac{u'_{e,inj}}{u'_B} \tag{A16}$$

where inequality (A15) was used and $\bar{\gamma} \equiv \int Q\gamma\, d\gamma / \int Q\, d\gamma$.

A.6. Toroidal vs. turbulent magnetic field

We assumed in the paper that magnetic field is dominated by the toroidal component. This assumption can be verified as follows. For $u'_{B,tor} >> u'_{B,turb}$, $u'_{B,tor} \simeq u'_{B,tot} \equiv u'_B$ and

$$u'_{B,tor} \simeq \frac{u'_B}{u'_{e,inj}} u'_{e,inj} = \eta_e \frac{u'_B}{u'_{e,inj}} u'_p(\bar{\gamma}_p - 1) \tag{A17}$$

For $u'_{B,turb} \simeq \eta_B u'_p(\bar{\gamma}_p - 1)$ this gives

$$\frac{u'_{B,tor}}{u'_{B,turb}} = \frac{\eta_e}{\eta_B}\frac{u'_B}{u'_{e,inj}} \tag{A18}$$

Note that all formulas which involve a Doppler factor apply for 'mono-Doppler' sources only. In the case of conically diverging jets, the observed radiation is contributed by jet

portions moving relative to the line of sight at different angles and then analytical estimations differ significantly from numerical results. This in particular concerns the quantity $K_{\rm e}$ because of its strong dependence on $\mathcal{D}$. However, for $\theta_{obs} \sim \theta_j \sim 1/\Gamma_j$, still reasonable analytical estimates are achievable if using $\mathcal{D} = 1.5\Gamma_j$, instead of $\mathcal{D} = \Gamma_j$.

B. The millimeter photosphere

Optically thin synchrotron spectrum in 3C454.3 and other quasar hosted blazars is produced by electrons in the fast cooling regime. In this regime an electron distribution is steepened due to radiative losses, and for a single-power-law injection function, $Q \sim \gamma^{-p}$, the electrons reach a distribution with the index $s = p + 1$. Below we provide estimation of the millimeter photosphere distance, assuming $p = 2$. For such a source the synchrotron-self absorption opacity $\tau(\nu'_{abs})$ is at $\nu'_{\rm a}$ equal to 1 for

$$R_{mm} = 2.7 \times 10^{-15} \frac{\nu_{\rm a}'^{7/2}}{c_n B'^{5/2}} \,[\rm cm] \tag{B1}$$

where $n_\gamma = c_n \gamma^{-3}$ is the electron density energy distribution.

Noting that

$$c_n = \frac{C_N}{V'} = \frac{C_N \Gamma_j^2 \mathcal{D}}{\pi r^3 (\Delta r/r)(\Gamma_j \theta_j)^2} \tag{B2}$$

where $C_N : N_\gamma = C_N \gamma^{-3}$, and that

$$N_\gamma = \frac{\int_\gamma Q \, d\gamma}{|\dot{\gamma}|_{tot}} \tag{B3}$$

where for $L_{ERC} > L_{syn}$

$$|\dot{\gamma}|_{tot} \simeq \frac{16 c \sigma_T \gamma^2 \Gamma_j^2 u_{ext}}{9 m_e c^2} \tag{B4}$$

we obtain, for $\theta_{obs}\Gamma_j = 1$ and $\Delta r = r$,

$$R_{mm} \simeq 1.9 \times 10^7 \frac{\mathcal{D}^{9/5}}{\Gamma_j^{7/5}} \frac{B'_0 r_0}{(u_{ext,in} r_{in}^2)^{2/5}} \frac{K_e^{2/5}}{[\nu_{\rm a,obs}(1+z)]^{7/5}} \,[\rm cm] \tag{B5}$$

and $r_{mm} = R_{mm}/\Gamma_j$. For $\nu_{\rm a,obs} = 3 \times 10^{11}$ Hz ($\lambda_{\rm a,obs} = 1$mm) and parameters of the Model 1 (see Table 1), this gives $R_{mm} \simeq 1.4 \times 10^{18}$ cm and $r_{mm} \simeq 2.8 \times 10^{19}$ cm.

REFERENCES

Appl, S., Sol, H., & Vicente, L. 1996, A&A, 310, 419

Arbeiter, C., Pohl, M., & Schlickeiser, R. 2002, A&A, 386, 415

Bach, U. et al. 2007, A&A, 464, 175, arXiv:astro-ph/0612149

Blandford, R. D., & Levinson, A. 1995, ApJ, 441, 79

Błażejowski, M., Sikora, M., Moderski, R., & Madejski, G. M. 2000, ApJ, 545, 107, arXiv:astro-ph/0008154

Celotti, A., Ghisellini, G., & Fabian, A. C. 2007, MNRAS, 375, 417, arXiv:astro-ph/0611439

Cleary, K., Lawrence, C. R., Marshall, J. A., Hao, L., & Meier, D. 2007, ApJ, 660, 117, arXiv:astro-ph/0612702

Dermer, C. D., & Schlickeiser, R. 1993, ApJ, 416, 458

Dermer, C. D., Schlickeiser, R., & Mastichiadis, A. 1992, A&A, 256, L27

Fuhrmann, L. et al. 2006, A&A, 445, L1, arXiv:astro-ph/0511829

Ghisellini, G., Foschini, L., Tavecchio, F., & Pian, E. 2007, ArXiv e-prints, 708, 0708.0617

Giommi, P. et al. 2006, A&A, 456, 911, arXiv:astro-ph/0606319

Gopal-Krishna, Wiita, P. J., & Dhurde, S. 2006, MNRAS, 369, 1287, arXiv:astro-ph/0603727

Gu, M., Cao, X., & Jiang, D. R. 2001, MNRAS, 327, 1111, arXiv:astro-ph/0104383

Hartman, R. C. et al. 1999, ApJS, 123, 79

Impey, C. D., Lawrence, C. R., & Tapia, S. 1991, ApJ, 375, 46

Jorstad, S. G., Marscher, A. P., Mattox, J. R., Wehrle, A. E., Bloom, S. D., & Yurchenko, A. V. 2001, ApJS, 134, 181, arXiv:astro-ph/0101570

Jorstad, S. G. et al. 2007, AJ, 134, 799, arXiv:astro-ph:0705.4273

Kataoka, J. et al. 2007, ApJ, arXiv:astro-ph/0709.1528, (in press)

Katarzyński, K., & Ghisellini, G. 2007, A&A, 463, 529, arXiv:astro-ph/0610801

Komissarov, S. S., Barkov, M. V., Vlahakis, N., & Königl, A. 2007, MNRAS, 380, 51

Komissarov, S. S., & Falle, S. A. E. G. 1997, MNRAS, 288, 833

Krichbaum, T. P., Lee, S. S., Lobanov, A. P., Marscher, A. P., & Gurwell, M. A. 2007, in Extragalactic Jets - Theory and Observation from Radio to Gamma-Ray, ed. T. A. Rector & D. S. De Young, ASP Conf. Series, arXiv:astro-ph/0708.3915

Laing, R. A. 1981, ApJ, 248, 87

McNaron-Brown, K. et al. 1995, ApJ, 451, 575

Moderski, R., Sikora, M., & Błażejowski, M. 2003, A&A, 406, 855, arXiv:astro-ph/0205228

Moderski, R., Sikora, M., Coppi, P. S., & Aharonian, F. 2005, MNRAS, 363, 954, arXiv:astro-ph/0504388, [Erratum: MNRAS, 364, 1488]

Moderski, R., Sikora, M., Madejski, G. M., & Kamae, T. 2004, ApJ, 611, 770, arXiv:astro-ph/0405229

Mukherjee, R. et al. 1997, ApJ, 490, 116

Nartallo, R., Gear, W. K., Murray, A. G., Robson, E. I., & Hough, J. H. 1998, MNRAS, 297, 667

Pian, E. et al. 2006, A&A, 449, L21, arXiv:astro-ph/0602268

Rawlings, S., & Saunders, R. 1991, Nature, 349, 138

Sikora, M., Begelman, M. C., Madejski, G. M., & Lasota, J.-P. 2005, ApJ, 625, 72, arXiv:astro-ph/0502115

Sikora, M., Begelman, M. C., & Rees, M. J. 1994, ApJ, 421, 153

Sikora, M., Błażejowski, M., Moderski, R., & Madejski, G. M. 2002, ApJ, 577, 78, arXiv:astro-ph/0205527

Sikora, M., & Madejski, G. 2000, ApJ, 534, 109, arXiv:astro-ph/9912335

Smith, P. S., Elston, R., Berriman, G., Allen, R. G., & Balonek, T. J. 1988, ApJ, 326, L39

Sokolov, A., Marscher, A. P., & McHardy, I. M. 2004, ApJ, 613, 725, arXiv:astro-ph/0406235

Spada, M., Ghisellini, G., Lazzati, D., & Celotti, A. 2001, MNRAS, 325, 1559, arXiv:astro-ph/0103424

Stevens, J. A., Robson, E. I., & Holland, W. S. 1996, ApJ, 462, L23+

Tavecchio, F. et al. 2002, ApJ, 575, 137, arXiv:astro-ph/0207157

Tavecchio, F., Maraschi, L., Wolter, A., Cheung, C. C., Sambruna, R. M., & Urry, C. M. 2007, ApJ, 662, 900, arXiv:astro-ph/0703359

Vercellone, S. et al. 2007, The Astronomer's Telegram, 1160, 1

Villata, M. et al. 2006, A&A, 453, 817, arXiv:astro-ph/0603386

Zhang, S., Collmar, W., & Schönfelder, V. 2005, A&A, 444, 767, arXiv:astro-ph/0508280

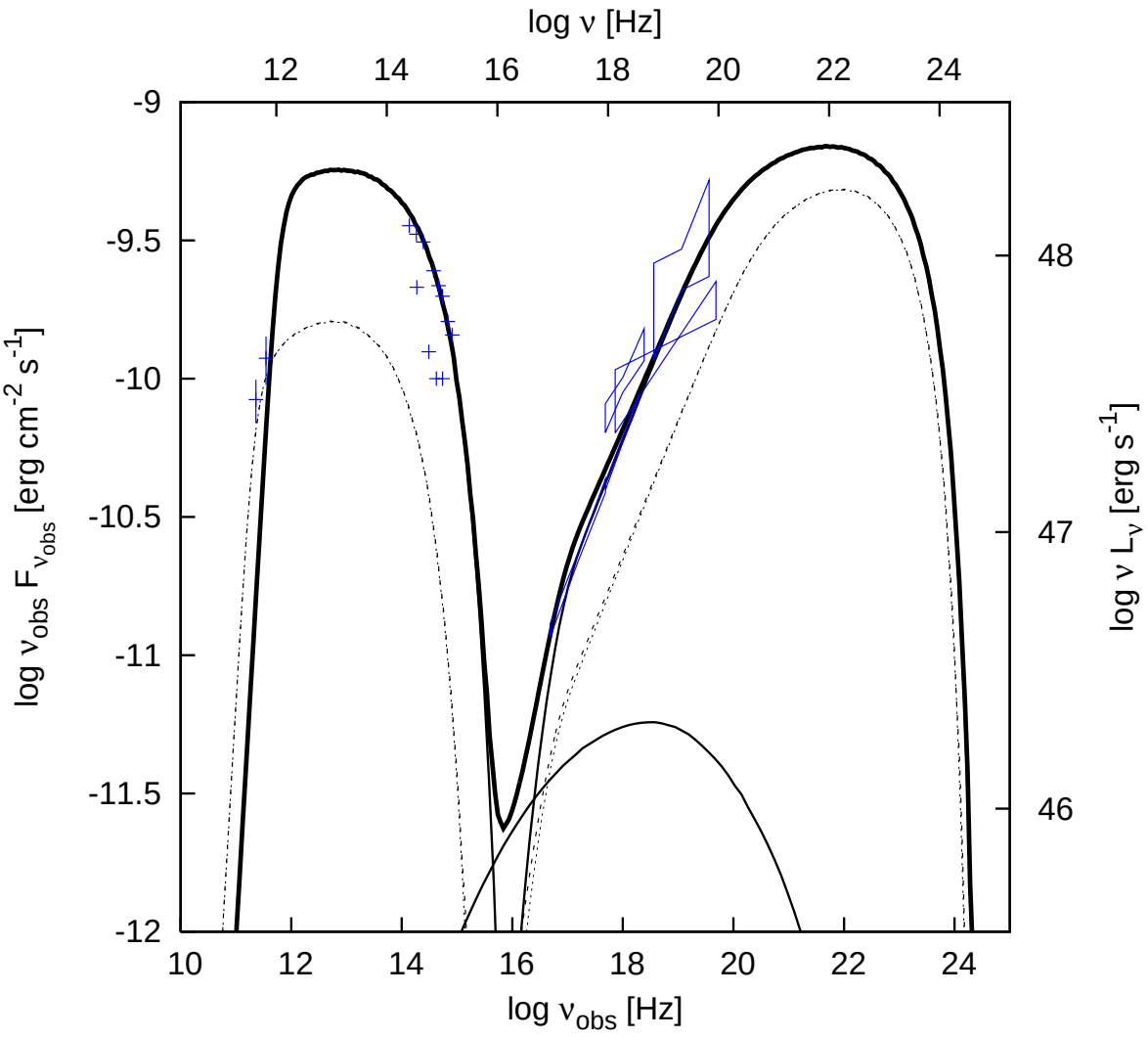

Fig. 1.— Data points show the broadband spectrum of 3C454.3 at the epoch of the optical peak during the 2005 outburst. Infrared data points at 1 mm and 3 mm and upper optical data points are from IRAM telescope and WEBT campaign, respectively, and were reported together with Chandra data in Villata et al. (2006). Lower optical data points from REM telescope and Swift data are taken from Giommi et al. (2006). Integral data are from Pian et al. (2006). Continuous lines show our preferred models obtained using the *BLAZAR* code (Moderski et al. 2003). Thick, solid line shows the model accounting for the broad-band data during the optical peak of the outburst (Model 1 in Table 1); the thin, solid lines indicate various components of the spectrum and illustrate that the SSC component is relatively weak. Dashed lines show the model spectrum produced at a distance twice as large as the thick solid line, and are intended to illustrate the emission at the millimeter photosphere (Model 2 in Table 1). Model parameters are given in Table 1.

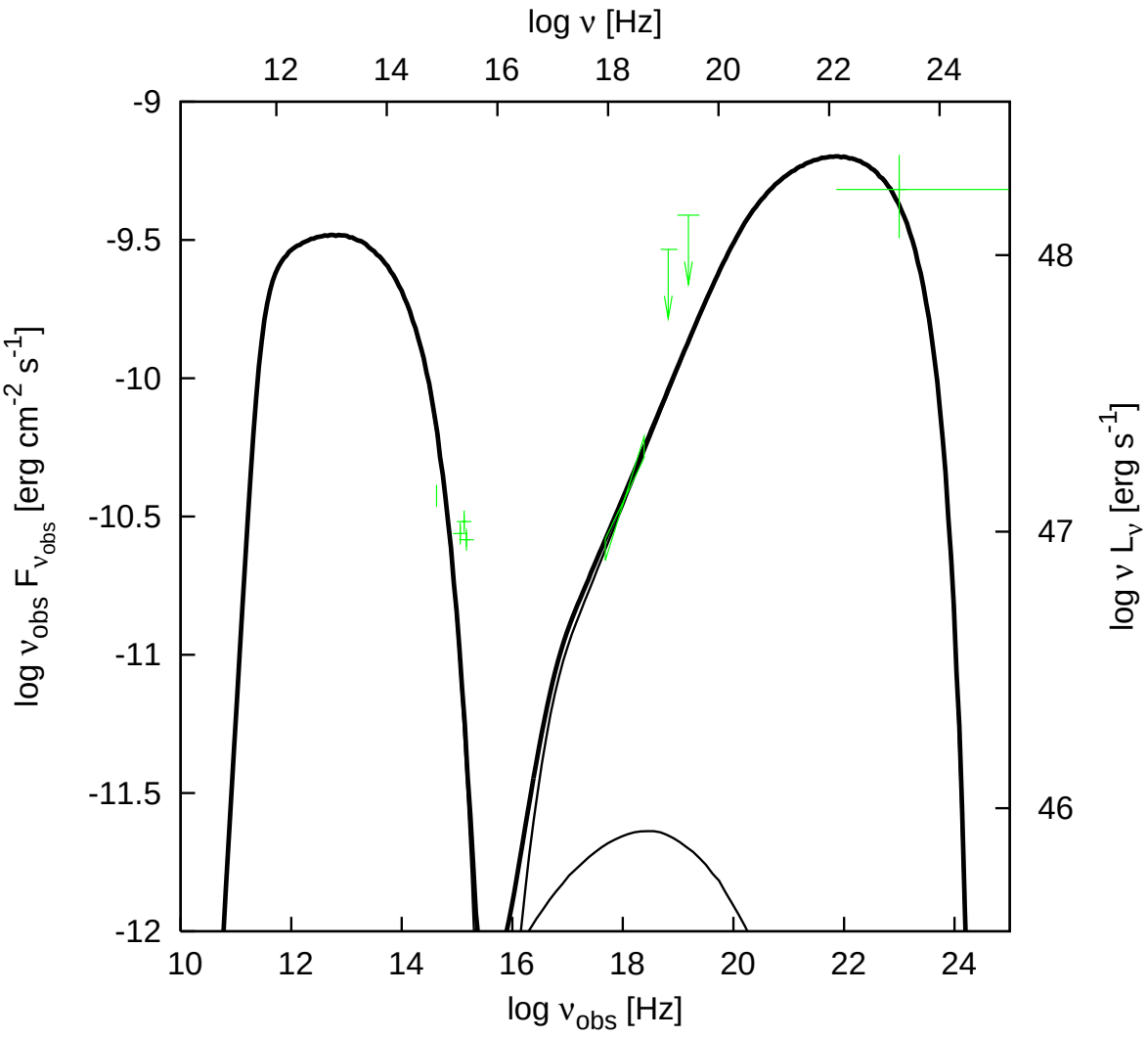

Fig. 2.— Broadband spectral observations of 3C454.3 during the 2007 outburst. Tuorla Observatory optical data point and Swift UV and X-ray data are taken from Ghisellini et al. (2007). Agile point comes from Vercellone et al. (2007). Model illustrated as a solid line has parameters given in Table 1 as Model 3.

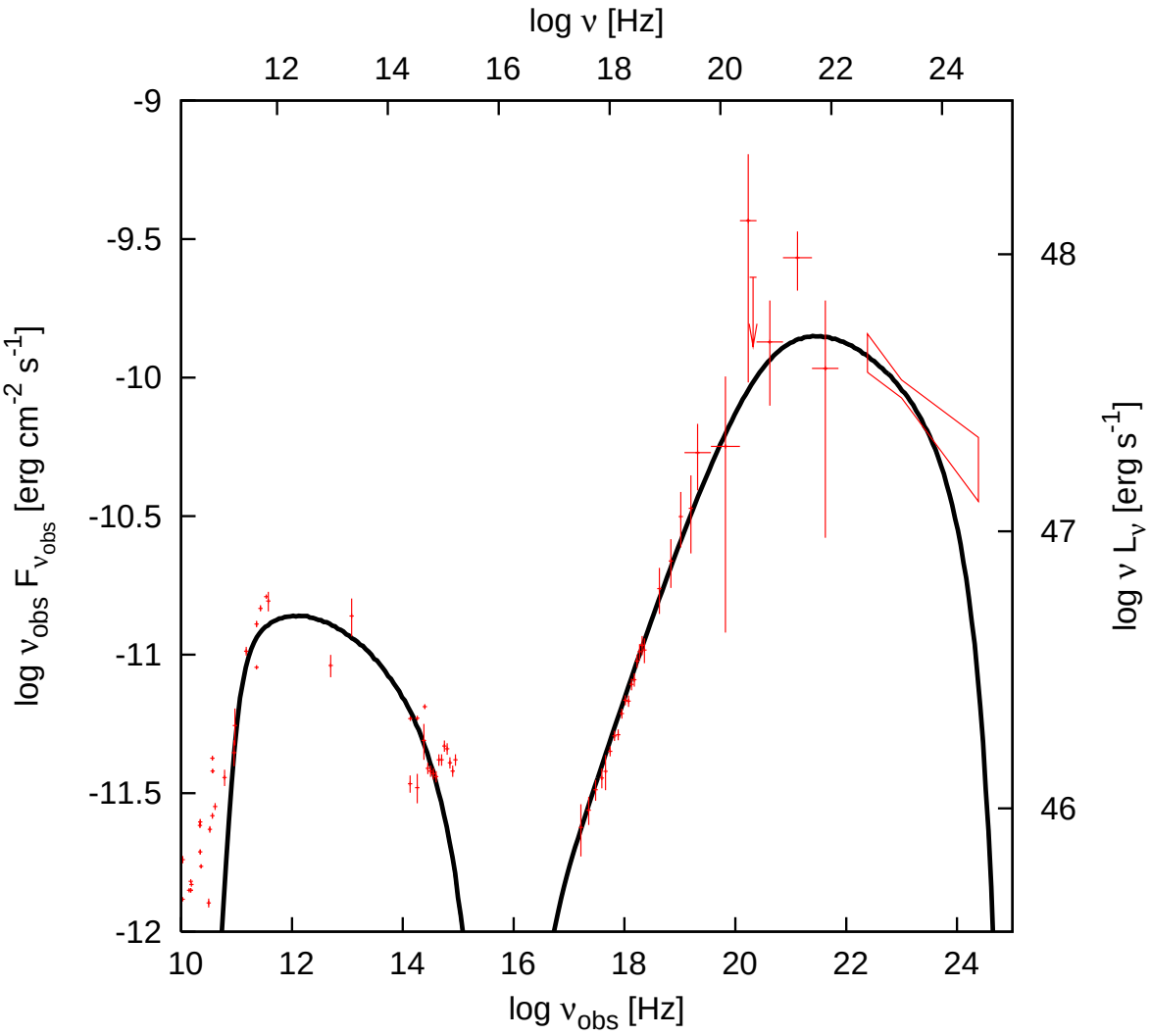

Fig. 3.— Broadband spectrum during the low state in the 'CGRO epoch'. All data points below 10^{16} Hz are from NASA Extragalactic Database. BeppoSAX data come from Tavecchio et al. (2002), while CGRO OSSE, Comptel and EGRET data are from McNaron-Brown et al. (1995), Zhang et al. (2005), and Hartman et al. (1999), respectively. Model accounting for those data, with parameters given in Table 1 (Model 4) is plotted as a solid line.

Table 1: The model parameters.

Parameter	Model 1	Model 2	Model 3	Model 4
$\gamma_{\rm min}$	1	1	1	1
$\gamma_{\rm br}$	—	—	—	80
$\gamma_{\rm max}$	4×10^3	4×10^3	4×10^3	9×10^3
p	2.0	2.0	2.0	1.7
q	2.0	2.0	2.0	2.5
$K_{\rm e}\,[{\rm s}^{-1}]$	3.0×10^{49}	1.5×10^{49}	2.3×10^{49}	3.0×10^{48}
$\Gamma_{\rm j}$	20	20	20	20
$\theta_{\rm j}$ [rad]	0.05	0.05	0.05	0.05
$\theta_{\rm obs}\,[{\rm rad}]$	0.05	0.05	0.05	0.05
$r_0=\Delta r_0\,[{\rm cm}]$	10^{19}	2×10^{19}	2×10^{19}	2×10^{19}
$B_0\,[{\rm G}]$	1.4	0.50	0.63	0.27
$r_{\rm in}\,[{\rm cm}]$	10^{19}	10^{19}	10^{19}	10^{19}
$u_{\rm IR}(r_{\rm in})\,[{\rm erg\,cm^{-3}\,s^{-1}}]$	1.24×10^{-4}	1.24×10^{-4}	1.24×10^{-4}	1.24×10^{-4}
$h\nu_{\rm IR}\,[{\rm eV}]$	0.34	0.34	0.34	0.34
$u'_{\rm e,inj}(2r_0)\,[{\rm erg\,cm^{-3}\,s^{-1}}]$	3.25×10^{-3}	4.06×10^{-4}	6.22×10^{-4}	1.95×10^{-4}
$u'_B(2r_0)\,[{\rm erg\,cm^{-3}\,s^{-1}}]$	1.95×10^{-2}	2.49×10^{-3}	3.95×10^{-3}	7.25×10^{-4}
$L_{\rm j}>L_B\,[{\rm erg\,s^{-1}}]$	7.35×10^{47}	3.75×10^{47}	5.96×10^{47}	1.10×10^{47}
$\bar\gamma_p-1<$	$0.17/\eta_e$	$0.16/\eta_e$	$0.16/\eta_e$	$0.26/\eta_e$
$\bar\gamma$	8.3	8.3	8.3	13.0
$n_e/n_p<$	$37.5/\eta_e$	$35.3/\eta_e$	$35.3/\eta_e$	$37.9/\eta_e$
$u'_{B_{tor}}/u'_{B_{turb}}$	$5.88\,\eta_e/\eta_B$	$6.25\,\eta_e/\eta_B$	$6.25\,\eta_e/\eta_B$	$3.72\,\eta_e/\eta_B$